Novel Elastomer-Dumbbell Functionalized POSS Composites: Thermomechanical and Morphological Properties

Steven Spoljaric, Antonietta Genovese, Robert A. Shanks

CRC for Polymers, Applied Sciences, RMIT University, Melbourne 3001, Australia

Received 2 November 2010; accepted 18 March 2011
DOI 10.1002/app.34518
Published online 28 July 2011 in Wiley Online Library (wileyonlinelibrary.com).

ABSTRACT: Nanocomposites consisting of poly(styrene-*b*-butadiene-*b*-styrene) (SBS) and polyhedral oligomeric silsesquioxanes (POSS) were prepared using a solvent dispersion method. Dumbbell-shaped POSS fillers were prepared using diacyl chlorides to bridge the POSS molecules. Infrared spectroscopy confirmed functionalization. Scanning electron microscopy revealed an increase in filler aggregation with concentration, with preferential phase selectivity. Polydispersity increased with filler concentration while *d* spacing was influenced by phase selectivity and domain-filler compatibility. Functionalized POSS improved thermal stability by imparting restrictions of SBS chain motions. Tensile stress–strain analysis revealed an increase in modulus, yield strength, and strain hardening with filler concentration, while creep deformation decreased and permanent strain increased with POSS content. Storage modulus, loss modulus, and glass transition temperature increased with filler content due to effective SBS–POSS interaction. Nanocomposite properties were influenced by filler concentration, the phase of the filler was dispersed throughout and the length of the alkyl "barbell" on the dumbbell-shaped POSS. © 2011 Wiley Periodicals, Inc. J Appl Polym Sci 123: 585–600, 2012

Key words: POSS; thermomechanical; functionalization; elastomer

INTRODUCTION

Functionalization involves the introduction of chemical functional groups onto a surface or substrate. Various chemical groups, including organic compounds,[1,2] fluorescent materials,[3] reactive dyes,[4,5] metals,[6] and magnetic compounds[7] have been bonded to surfaces such as carbon black, fumed silica, montmorillonite clays, and alumina. These hybrid materials show much potential for incorporation into polymer composites as a novel class of filler. By combining the specific functionality of the bonded chemical groups with the mechanical, thermal, or additional intrinsic properties of the surface/substrate, functionalized fillers provide potential for new materials and properties. One particular class of filler suitable for functionalization are polyhedral oligomeric silsesquioxanes (POSS, empirical formula $RSiO_{1.5}$). These hybrid molecules consist of a rigid inorganic core consisting of 8, 10, or 12 silicon atoms linked by oxygen atoms, with organic substituents attached at the corners of the silica cage. The central core is ceramic in nature, providing thermal stability and rigidity, while the organic groups compatibilize the molecule.[8] First synthesized in 1946 by Scott,[9] POSS have begun to attract serious attention as a filler material within the last 10–15 years, encouraged by the significant improvement in composite properties the fillers provide.

A variety of functional groups have been bonded directly onto POSS molecules, including organic groups,[10] metals,[11] and fluorescent emitters.[12,13] The possibility of introducing these molecules is encouraged by the commercial availability of POSS with pre-existing reactive groups, such as trisilanol or amines.[14] In addition, POSS molecules with various architectures and molecular shapes have been prepared, including pendant,[15] bead,[16] tadpole,[17] and star[18,19] structures. Several of these shape-functionalized POSS have been incorporated into network structures or grafted onto polymer chains to prepare nanocomposites[20–23] with noticeable enhancements in glass transition temperature, thermal stability, and mechanical properties. Another specific architectural structure is dumbbell-shaped (telechelic) POSS, consisting of two POSS "weights" connected chemically by an alkyl, polymer, or similar chain "barbell." These structures have received relatively little attention,[24,25] despite exhibiting enhanced thermal stability, solubility, and film-forming properties. Mather and coworkers[26–28] have synthesized telechelic polymers consisting of a poly(ethylene glycol) bridges with POSS bonded to the chain end groups, observing

Correspondence to: R. Shanks (robert.shanks@rmit.edu.au).
Contract grant sponsors: CRC.

changes in crystallization behavior, thermal degradation, and surface properties. However, there are no reported cases of dumbbell-shaped POSS fillers being incorporated into polymer matrices.

Block copolymers have received much academic and industrial attention since the early 1960s, due to low production costs and unique intrinsic properties. In recent times, focus has shifted toward nanotechnology applications, mainly due to the ability of these polymers to form self-assembled domains on the nanometre scale and the ease of which domain size/shape can be manipulated by altering the molecular weight or block concentration.[29,30] This allows for potential in a number of applications, including biomedical, membrane formation, electronics, and information technology.[31] A popular choice of block copolymer is poly(styrene-*b*-butadiene-*b*-styrene) (SBS), a linear triblock-elastomer consisting of hard, glassy polystyrene and soft, rubbery polybutadiene segments. Pure SBS is seldom used in applications, often being compounded with polystyrene to enhance mechanical properties and reduce production costs.[32] SBS nanocomposites have received much attention in recent years, with fillers including silica, carbon black, and montmorillonite clays being incorporated into the SBS matrix.[33–35] While enhancements in composite properties have been achieved, molecular-level dispersion has been difficult, due to poor matrix–filler compatibility. This can lead to further complications when the objective is to disperse fillers within a particular phase. The incorporation of POSS into SBS has been limited.[36–38] Furthermore, SBS-POSS nanocomposites are usually prepared with grafting reactions. This provides the opportunity of preparing these nanocomposites using physical blending techniques and to determine whether adequate filler dispersion can be achieved. In addition, the benefit of dispersing the POSS throughout a copolymer, such as SBS, will allow the phase preference of the filler to be observed, due to the compatibilising organic "R" groups on the POSS molecule.

The aim was to synthesis SBS-POSS nanocomposites via a physical blending process, where the POSS will favor a specific phase of the polymer matrix and enhance composite properties, with the different functionalized POSS structures exhibiting various influence on material properties. Objectives included preparation of dumbbell-shaped POSS using diacyl chlorides, preparing SBS-POSS nanocomposites using a solvent dispersion technique, and characterizing the thermomechanical, viscoelastic, thermal, optical, and morphological properties of the nanocomposites.

EXPERIMENTAL

Materials

Poly-*co*-(styrene-*b*-butadiene-*b*-styrene) (SBS) used as matrix material was Kraton D-1102 (Kraton Polymers LLC). It is a pure, linear triblock copolymer with 29.5·wt % bound styrene and a density of 0.938 g cm^{-3}. Two types of POSS were obtained from Hybrid Plastics, Hattiesburg, USA; trisilanolheptisobutyl (SO1450) and trisilanolheptaphenyl (SO1458).

Aminosilane-treatment of POSS

TrisilanolPOSS (6.32 mmol) and 3-aminopropyltriethoxysilane (6.5 mmol) were dispersed in 40 mL solvent and stirred for 24 h. TrisilanolphenylPOSS was stirred in toluene and cooled using an ice bath while trisilanolisobutylPOSS was dispersed in tetrahydrofuran (THF) and stirred at room temperature. The solution was poured into 100 mL acetonitrile and stirred for 10 min, before being suction filtered, washed with methanol and deionized water and dried in a vacuum oven at 75°C overnight.

Preparation of dumbbell-POSS

Aminosilane-treated POSS (2.07 mmol) and triethylamine (2.31 mmol) were dissolved in 50 mL THF and stirred under nitrogen for 20 min at room temperature. Sebacoyl or adipoyl chloride (1 mmol) was added dropwise and the solution was stirred overnight. After evaporating the solvent, the dumbbell-shaped POSS was washed with methanol and dried in a vacuum oven at 25°C overnight. The complete preparation of the dumbbell-POSS fillers is shown in Figure 1.

Preparation of SBS-POSS nanocomposites

SBS was dispersed in 150 mL of dichloromethane and stirred for 1 h at 25°C, until the polymer was completely dissolved. Functionalized POSS was added to the solution and subjected to ultrasonic disruption (10 min, 25°C, 20 kHz) to ensure even distribution of the filler throughout the matrix. The solution was poured into an excess of cold methanol to precipitate the nanocomposite material and to restrict filler migration. The product was isolated using suction filtration and dried in a desiccator overnight. Films for subsequent use were prepared using a heated press (IDM Instruments, model number L0003-1). Films were heated to 150°C, 6 t applied, held for 2 min and cooled to ambient.

Characterization of materials

Fourier transform infrared spectroscopy

A Perkin–Elmer Spectrum 2000 FTIR spectrometer working in diffuse reflectance spectroscopy (DRIFTS) mode was used to characterize the molecular vibration of the functional groups in the POSS derivatives. Anhydrous potassium bromide (KBr) was used as dispersing material and all spectra were scanned

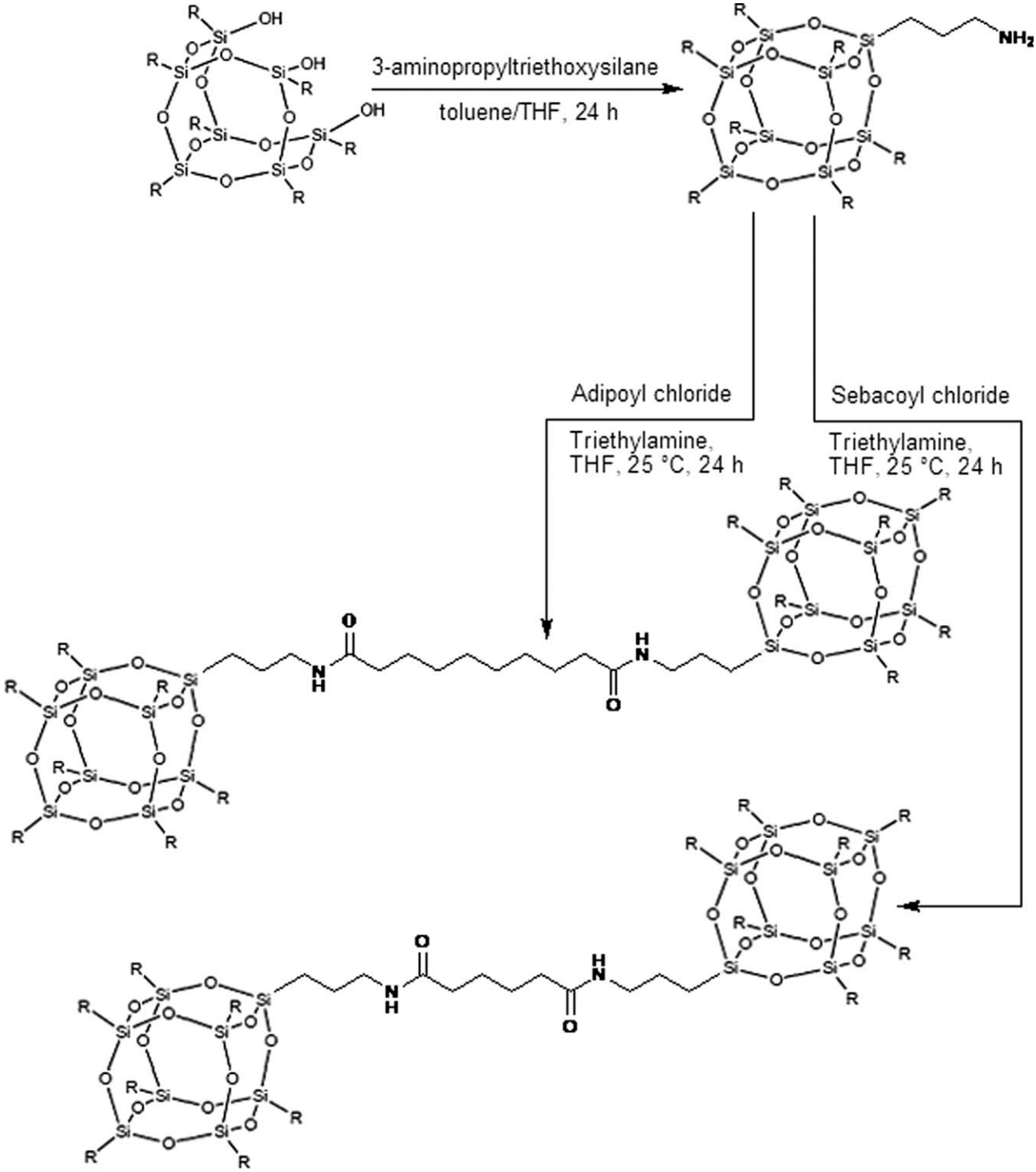

Figure 1 Preparation of dumbbell-POSS.

within the range 400–4000 cm^{-1}, with a total of 20 scans and a resolution of 8 cm^{-1}.

Scanning election microscopy

Scanning electron microscopy (SEM) images of the nanocomposites were taken using a FEI Quanta 200 environmental scanning electron microscope (ESEM) operating at 30 kV. Composites with average dimensions $\sim$ 4.00 $\times$ 4.00 $\times$ 0.70 mm^3 were mounted to the specimen holder using carbon tape.

Small angle X-ray scattering

A Bruker AXS Nanostar was used to study the morphology of the polymer composites. A Cu X-ray

source ($\lambda = 0.1542$ nm) was generated at kV = 40 and mV = 35. The distance from the sample to detector was 106 cm.

Thermogravimetry

A Perkin–Elmer TGA-7 thermogravimetric analyzer with TAC-7/DX thermal analysis controller was used to analyze the thermal stability of the composites. Samples of $\sim$ 10 mg were heated to 850°C at 20°C min^{-1} in an inert environment provided by a 20 mL min^{-1} nitrogen purge. The mass loss was recorded as a function of temperature.

Ultraviolet–visible spectroscopy

A Varian 50 Bio UV visible spectrophotometer was used to analyze the absorbance and transmittance of the nanocomposites. Samples were scanned from 800 to 200 nm using a dual beam at a scan rate of 1008 nm min^{-1}.

Thermomechanical analysis

Stress-strain (dynamic force-thermomechanometry, df-TM) analysis was performed using an Instron Universal Testing Instrument, Model 4465 with a 5000-kN load attached, while a TA Instruments Q800 Dynamic Mechanical Analyzer in tensile mode was used for creep-recovery (static force-thermomechanometry, sf-TM) and modulated force-thermomechanometry (mf-TM) analysis.

Stress–strain.. Test samples were cut from the pressed films using dumbbell-shaped test bars according to ASTM D638 - 97, specimen type IV. A strain rate of 50 mm min^{-1} was applied to each sample at ambient temperature. Results presented are the average of five measurements.

Creep-recovery.. Samples with dimensions of $\sim 12.80 \times 4.00 \times 0.70$ mm^3 were subjected to an applied stress of 0.5 MPa for 60 min, followed by a recovery period of 240 min with 0.01 MPa applied stress. The applied stress chosen was within the linear viscoelastic region of all the nanocomposites. Tests were conducted at ambient temperature (30°C) and all results presented are the average of triplicate measurements. The four-element model of Maxwell and Kelvin-Voigt [Fig. 2(a)] was used to interpret the creep component. The springs correspond to elastic sections with moduli E_1 and E_2, while the dashpots represent the viscosity (η_1, η_2). The overall deformation of the model is given in Eq. (1).

$$\varepsilon(f) = (\sigma_0/E_1) + (\sigma_0/\eta_1) + (\sigma_0/E_2)(1 - e^{-t/(\eta_2/E_2)}) \quad (1)$$

The stretched exponential function of Kohlrausch, Williams, and Watts[39] (KWW) was used to interpret the recovery behavior and is given in Eq. (2);

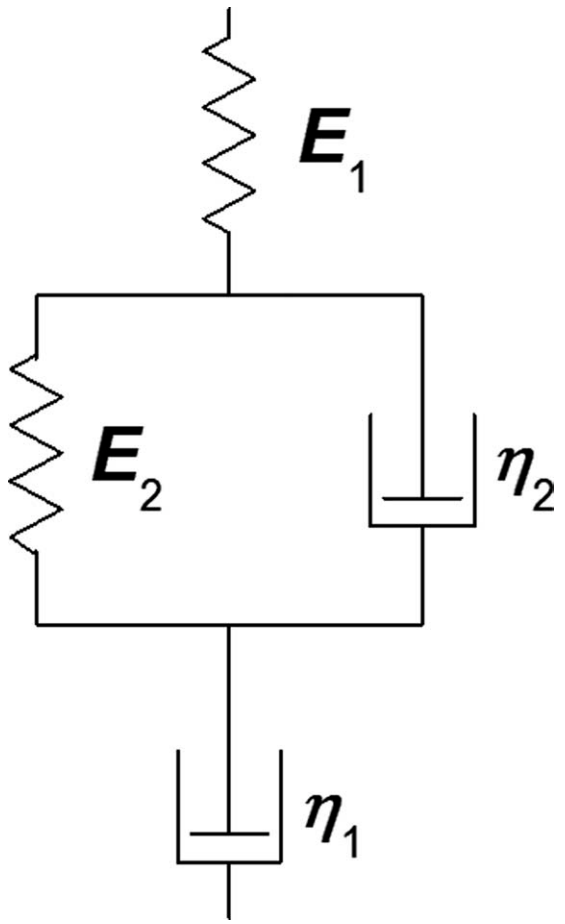

Figure 2 The four-element model.

$$\phi = A \exp^{-(t/\tau)^{\beta}} \quad (2)$$

where A is the pre-exponential coefficient, t is time, τ is the retardation time, and β is the nonlinearity coefficient ($0 < \beta < 1$). Placing the four-element model (Fig. 2) in series provides a model of viscoelastic recovery behavior with a distribution of relaxation times.[40] Each set of springs a dashpots corresponds to a characteristic relaxation time.

Modulated force-thermomechanometry.. Modulated force-thermomechanometry (mf-TM) analysis was conducted using a static force of 500 mN, modulated force of 100 mN, and frequency of 1 Hz. The storage modulus (E'), loss modulus (E''), loss tangent (tan δ), and associated glass transition (T_g) temperatures of the films were measured as a function of temperature from -100 to $+$ 110°C at a heating rate of 2°C min^{-1}.

Nomenclature of materials

The nomenclature of the nanocomposites is as follows: SBS-*x*POSS-*y* *z*; where *x* corresponds to the compatibilizing "R" groups on the POSS cage corners (ib = isobutyl, ph = phenyl), *y* is the diacyl

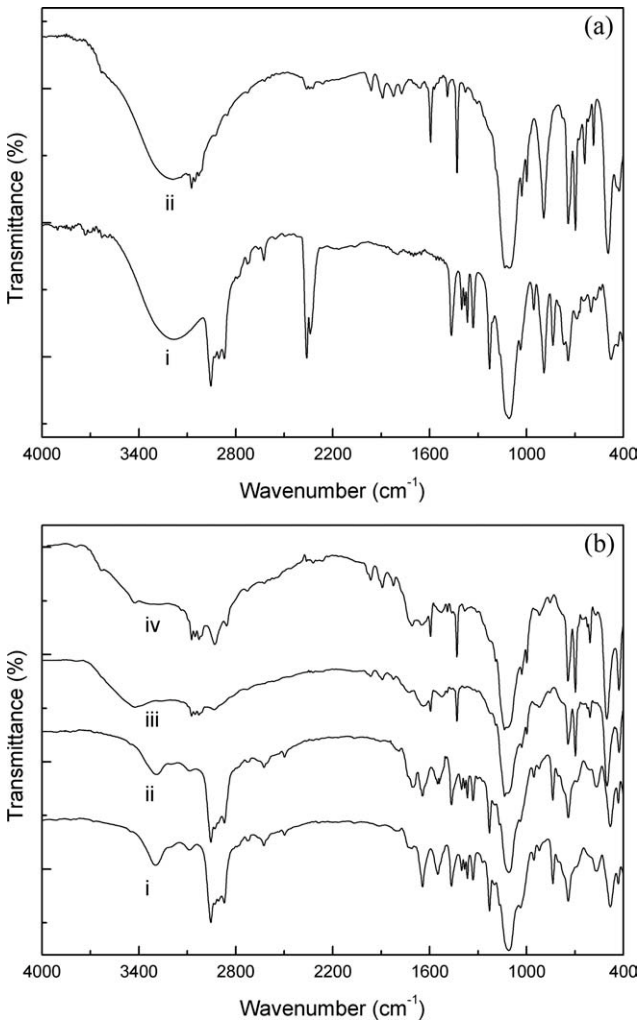

Figure 3 (a) Infrared spectrographs of untreated POSS; (i) TrisilanolisobutylPOSS, (ii) TrisilanolphenylPOSS, (b) infrared spectrographs of functionalised POSS; (i) isobutyl-POSS-adichl, (ii) isobutylPOSS-sebchl, (iii) phenylPOSS-adichl, (iv) phenylPOSS-sebchl.

chloride "barbell" used to bridge the POSS molecules (adichl = adipoyl chloride, sebchl = sebacoyl chloride), and z is the concentration of filler within the SBS matrix (%·wt).

RESULTS AND DISCUSSION

Fourier transform infrared spectroscopy

FTIR spectroscopy was used to confirm the chemical structure formed by the reaction of POSS and the diacyl chlorides and to determine whether bonding between the respective molecules was achieved. The infrared spectra of the untreated POSS are shown in Figure 3(a). The pure POSS show several bands characteristic of their structure: 3154 cm^{-1} (hydroxyl (OH) stretching vibrations), 1100 and 890 cm^{-1} (Si—O—Si and SiOH stretching vibrations). TrisilanolphenylPOSS displays bands at 1594, 1490, and 1430 cm^{-1}, corresponding to vibrational stretching of the C=C bonds within the phenyl "R" groups. The three bands in this region confirm the presence of a conjugated phenyl system. Other bands corresponding to the trisilanolphenylPOSS structure include 3070 cm^{-1} (sp^2 CH stretching vibrations), 696 and 740 cm^{-1} (C—H bending vibrations). TrisilanolisobutylPOSS exhibits strong bands at 2950, 2900, and 2868 cm^{-1}, corresponding to vibrational stretching of the CH_3, CH_2, and CH groups of the isobutyl "R" groups. Other peaks specific to isobutyl include those at 1462, 1400, 1366, and 1328 cm^{-1}, correlating to CH_2 and CH_3 bending vibrations and deformation.

The infrared spectra of the functionalised dumbbell-POSS are shown in Figure 3(b). For all functionalized POSS, a noticeable reduction in peak size is noticed at 3154 cm^{-1}. This indicates a reduction in the number of OH groups on the POSS molecules, suggesting that bonding has occurred between the trisilanol group and 3-aminopropyltriethoxysilane used to treat the trisilanolPOSS. This was confirmed by the presence of new peaks at 3264 cm^{-1} (*N*—H vibrations). The formation of amide bonds between the amine-treated POSS and diacyl chlorides was confirmed by the presence of two peaks at 1638 and 1536 cm^{-1}. These bands correspond to Amide I (C=O stretching) and Amide II (*N*—H bending) vibrations, respectively.[41] Dumbbell-phenylPOSS fillers displayed new peaks at 2902 and 2848 cm^{-1} which are attributed to CH_2 vibrations of the alkane "barbell" chains. These vibrations could also contribute to dumbbell-isobutylPOSS CH_2 vibrations at 2950, 2900, and 2868 cm^{-1}, in addition to isobutyl group contributions. The lack of new peaks at 800–700 cm^{-1} (C—Cl stretching),[42] 930 cm^{-1} (CO—Cl stretching)[43] or 1815–1770 cm^{-1} (acyl halide C=O vibrations)[42] suggests that there is no unreacted sebacoyl or adipoyl chloride remaining and that reactions occurred at both acyl chloride groups. These observations strongly encourage that sufficient interaction and bonding has occurred between the treated trisilanol POSS and diacyl chlorides and that the desired dumbbell-shape molecule was formed.

Scanning electron microscopy

Scanning electron microscopy (SEM) was employed to investigate the morphology and extent of filler dispersion within the nanocomposites. The micrographs are presented in Figure 4. Incorporation of up to 5%·wt POSS into the SBS resulted in a relatively uniform distribution of filler throughout the matrix, with POSS clustering into small agglomerates with an average diameter of $\sim$ 0.5–1.5 μm. As the concentration of POSS increased, so did the occurrence of agglomeration, ranging from few small instances at 5·wt % [Fig. 4(a)] to the formation of

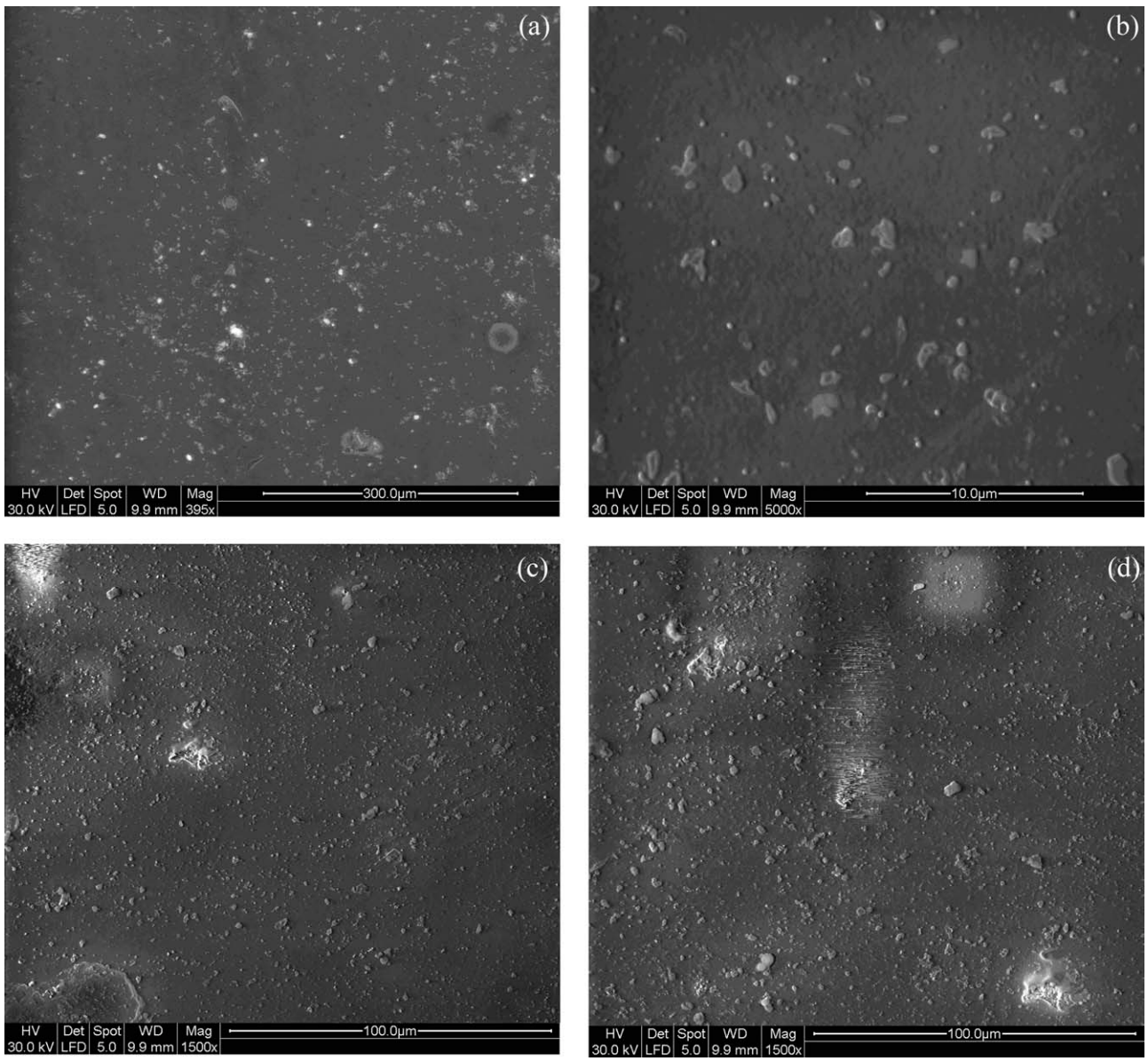

Figure 4 Scanning electron micrographs of SBS-POSS nanocomposites; (a) SBS-ibPOSS-adichl 5, (b) SBS-ibPOSS-adichl 20, (c) SBS-ibPOSS-sebchl 10 (d) SBS-phPOSS-sebchl 10.

large agglomerates at 20·wt % with average diameters of ~ 11 μm [Fig. 4(b)]. Despite utilizing ultrasonic disruption to discourage filler clustering and solvent precipitation to "suspend" the filler in a desired spatial arrangement, the micrographs indicate that at POSS concentrations greater than 5·wt %, interactions between the functionalized POSS nanoparticles are quite strong and can withstand physical methods used to encourage particle separation. These interactions are usually in the form of Coulombic and van der Waals forces.

Figure 4(c,d) display the micrographs of SBS-ibPOSS-sebchl 10 and SBS-phPOSS-sebchl 10, respectively. Incorporation of 10·wt % ibPOSS-sebchl gave an even distribution of filler throughout the matrix, with small clusters of ~ 2–3 μm. Conversely, addition of phenylPOSS at the same concentration and functionalized with the same diacyl chloride leads to an increase in the development of agglomeration, with larger clusters of ~ 5–8 μm occurring. This behavior is attributed to the corner "R" groups on the silsesquioxane cages, which determine phase compatibility and, therefore, morphology. The bulk of the SBS matrix used consists of polybutadiene (~ 70.5·wt %), providing isobutylPOSS groups a relatively large volume to disperse throughout and occupy. This was in contrast to phenylPOSS, which by comparison has a significantly smaller volume of polymer (styrene phase) to occupy, leading to increased interactions between the POSS molecules due to their proximity. This leads to the formation of larger agglomerates within the fewer styrene

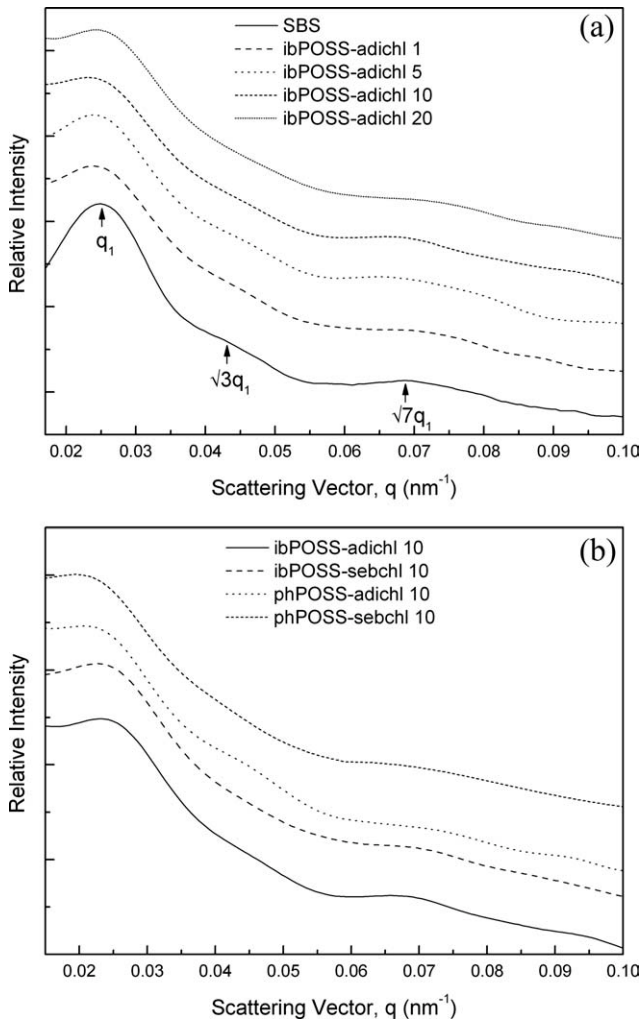

Figure 5 One-dimensional SAXS profiles; (a) SBS and SBS-ibPOSS-adichl composites, (b) 10·wt % filled composites.

domains available. Adipoyl and sebacoyl chloride-functionalized POSS exhibited similar distribution behavior, with the degree of aggregation and particle diameter being primarily influenced by the phase throughout which the fillers were dispersed (via the corner "R" groups).

Small angle X-ray scattering

Figure 5 shows the one-dimensional small angle X-ray scattering (SAXS) profiles of SBS and selected nanocomposites, while material characteristics derived from SAXS data are summarized in Table I. The relative intensity was plotted against the magnitude of the scaling vector (q). As shown in Figure 5(a), the scattering pattern of pure SBS displayed three distinct maxima (q_{max}) at $q = 0.026$, 0.042, and 0.069 nm^{-1} that were denoted q_1, $\sqrt{3}q_1$, and $\sqrt{7}q_1$, respectively, This sequence of Bragg peaks is typical of a hexagonicaly-packed cylinder morphology, which was expected of SBS with a polystyrene concentration of 29.5·wt %.[38] Incorporation of ibPOSS into the SBS matrix had no influence on the location of the peak at $q = 0.026$ nm^{-1}, suggesting the SBS-ibPOSS composites exhibit a similar d spacing value of $\sim$ 241 nm ($d = 2\pi/q_{max}$). This indicates that ibPOSS does not change the cylindrical structure of SBS. Although peak location remained fairly constant, peak intensity decreased with filler concentration. This was especially noticeable at filler loadings of 10 and 20·wt %, where the peaks at 0.042 and 0.069 nm^{-1} become broader and tapered. Fu et al.[38] observed a similar decrease in peak intensity and lack-of-change in peak location in SBS composites grafted with isobutylPOSS. The behavior was attributed to isobutylPOSS inhibiting the long-range order of polystyrene domains, restricting their packing ability. Conversely, phenylPOSS composites experienced a q_1 shift toward smaller angles (larger d spacing values) with increasing concentration, exhibiting maximum d spacing values at concentrations of 10·wt %. This behavior is indicative of an increase in the interdomain distance between polystyrene domains. To quantify this behavior, the interdomain distance (D) was calculated using Eq. (3)[44];

$$D = \sqrt{4/3} \bullet d_{100} \tag{3}$$

where d_{100} corresponds to the d spacing value of the primary peak. Pure SBS yielded an interdomain distance of 278 nm. As summarized in Table I, isobutylPOSS composites displayed little variation in D while materials reinforced with phenylPOSS exhibited an increase in D with filler content, reaching maximum values of 329 and 340 nm for SBS-phPOSS-adichl 10 and SBS-phPOSS-sebchl 10, respectively. Incorporation of phenylPOSS into SBS

TABLE I
SAXS Characteristics of SBS and SBS-POSS Composites

Material	d Spacing (nm)	D (nm)	$R_{cylinders}$ (nm)
SBS	241	278	328
ibPOSS-adichl-1	253	292	345
ibPOSS-adichl-5	253	292	345
ibPOSS-adichl-10	245	283	334
ibPOSS-adichl-20	245	283	334
ibPOSS-sebchl-1	245	283	334
ibPOSS-sebchl-5	253	292	345
ibPOSS-sebchl-10	250	289	341
ibPOSS-sebchl-20	253	292	345
phPOSS-adichl-1	253	292	345
phPOSS-adichl-5	268	310	365
phPOSS-adichl-10	285	330	389
phPOSS-adichl-20	276	318	375
phPOSS-sebchl-1	261	301	355
phPOSS-sebchl-5	275	318	375
phPOSS-sebchl-10	295	340	401
phPOSS-sebchl-20	285	330	389

leads to the fillers dispersing throughout the polystyrene domains, facilitated by the phenyl compatibilizing groups. This results in expansion of the cylindrical polystyrene domains, leading to the centers of the cylinders becoming further apart from one another. The extent of domain growth was determined by calculating the radius of the cylinders ($R_{cylinders}$) using Eq. (4)[45];

$$R_{cylinders} = [d_{100}(3^{1/2}\phi_B/2\pi)^{1/2}] \quad (4)$$

where φ_B is the volume fraction of the minor phase. IsobutylPOSS exhibited relatively little influence on $R_{cylinders}$, while the incorporation phenylPOSS expanded the radius of the polystyrene domains. However, at filler loadings of 20·wt % d spacing, D and $R_{cylinders}$ decreased. Given the limited volume available for phenylPOSS to disperse throughout, higher filler loadings will increase the probability of phenylPOSS dispersing in polybutadiene domains and forming agglomerates. Therefore, we can conclude that at filler concentrations up to and including 10·wt %, phenylPOSS expands the cylindrical polystyrene domains, resulting in the interdomain distance increasing. As filler loading is increased past 10·wt %, phenylPOSS is likely to be dispersed throughout both polybutadiene and polystyrene phases, leading to a reduction in interdomain distance, cylinder radius and subsequent segregation between hard and soft domains.

All composites displayed peak broadening with increasing filler concentration. Among the factors which influence peak breadth is polydispersity,[37] particularly in polymer composites since system polydispersity increased with filler concentration. As shown in Figure 5(b), phenylPOSS composites exhibited broader primary peaks (q_1) than their isobutylPOSS counterparts, in particular at filler loadings of 10 and 20·wt %. As mentioned previously, POSS inhibits the long-range order of polystyrene domains, restricting their packing ability. The increased domain radii and interdomain distance due to the incorporation of phenylPOSS will increase the difficulty of achieving hexagonal-closed packing, reducing material regularity. At concentrations of 20·wt %, segments of phenylPOSS within the polybutadiene phase may further hinder the packing process. Hence, phenylPOSS composites displayed broader peaks than their isobutyl counterparts.

UV–visible spectroscopy

The influence of the functionalized-POSS fillers on optical properties was analyzed using UV–visible spectroscopy. In addition to thermal resistance and softness, optical clarity is an crucial property of developmental thermoplastic elastomers.[46] The incorporation of micro-sized particles as fillers into a polymer matrix absorbs and scatters light, reducing optical clarity.[47] Scattering can be reduced by encouraging particle dispersion and matrix-filler interaction, with the optimum filler diameter being $\sim$ 200 nm (half the wavelength of visible light). The transmittance spectra of various SBS-POSS nanocomposites are shown in Figure 6(a). Incorporating POSS within the SBS matrix caused a reduction in transmittance, which continued to decrease with filler concentration. PhenylPOSS composites displayed lower transmittance values than their isobutylPOSS counterparts for the same concentration. Although all materials were subjected to ultrasonic disruption in an attempt to achieve this level of dispersion, the effect of phase preference needs to be considered. The SBS matrix is a block copolymer composed of $\sim$ 70.5·wt % polybutadiene and 29.5·wt % polystyrene. Since the amount of butadiene (continuous, rubbery block) phase is significantly higher than styrene (glassy block), isobutylPOSS particles with an

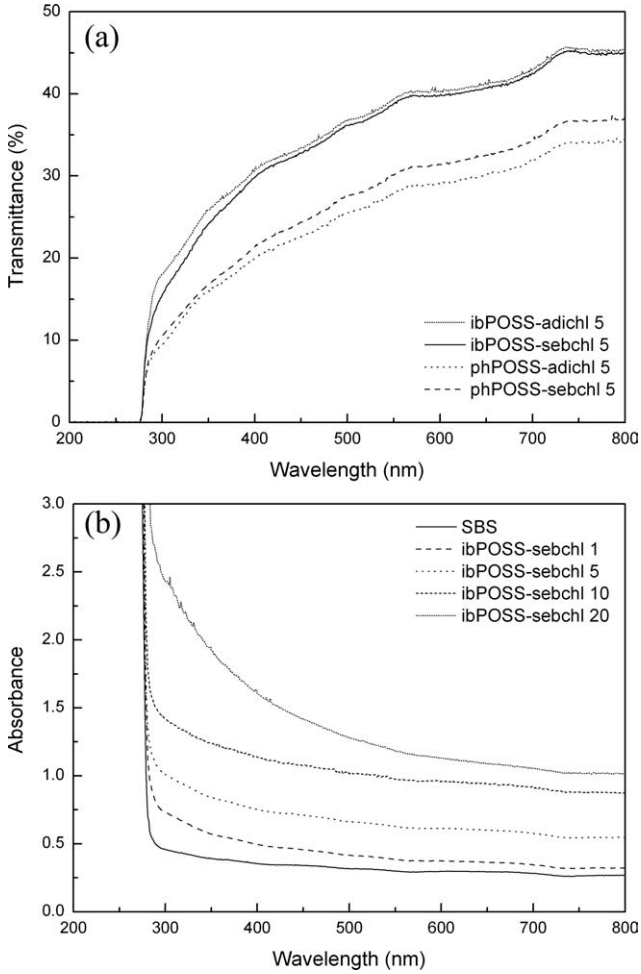

Figure 6 (a) Transmittance spectra of composites 5·wt % filled POSS composites, (b) absorbance spectra of SBS-ibPOSS-sebchl composites.

affinity for the rubber phase have greater volume for dispersion. In contrast, POSS with a preference for the polystyrene domains have a more constrained local environment to disperse throughout and will increase the likelihood of aggregate formation. This contrast in dispersion and subsequent light scattering properties was confirmed using SEM (refer Fig. 4).

The UV absorbance spectra of SBS-ibPOSS-sebchl nanocomposites are shown in Figure 6(b). The intensity of the UV absorbance increased with POSS concentration, correlating to the increase in filler-agglomerates and number of POSS particles available to scatter UV light. Minimal differences were observed between composites containing adipoyl and sebacoyl chloride-functionalised POSS, due to scattering being influenced by the degree of dispersion rather than particle geometry/flexibility.[48] The addition of functionalized-POSS caused the absorption spectra to shift toward longer wavelengths, with the inflection onset shifting towards longer wavelengths with concentration. This suggests that POSS acts as a physical crosslink, reducing the amount of effective energy within the polymer and shifting the spectra.[49]

Thermogravimetry

The mass loss versus temperature curves of pure SBS and nanocomposites are shown in Figure 7. The decomposition of SBS shows one degradation step at $\sim$ 467°C. The thermal degradation mechanism of SBS consists of two main processes, namely chain scission and crosslinking.[50] As seen in Figure 7(a), incorporation of functionalised POSS into the SBS matrix increased the temperature at which the maximum rate of degradation occurs (T_d), with nanocomposites containing 1·wt % POSS yielding T_d values ranging from 469 to 472°C. T_d continued to increase with filler content, reaching a maximum of 495°C in SBS-phPOSS-adichl 20. This behavior is characteristic of the thermal stability of POSS which stems from its silicon-oxygen structure. A proposed mechanism of thermal reinforcement is that POSS molecules restrict polymer chain motions, due to polymer–filler interactions or by the large inertia exhibited by segments of polymer containing POSS.[20,51] The compatibilizing organic groups on the POSS encourage this interfacial interaction, allowing thermal reinforcement to be achieved. The POSS can provide the most "torturous path" for thermal degradation, lengthening the degradation process and increasing thermal stability.

At filler concentrations of 1–5·wt % (agglomerate diameter generally <2 μm), nanocomposites containing isobutylPOSS showed higher T_d values than their phenylPOSS counterparts. The thermal stability of SBS is dependent on the sensitivity of the double

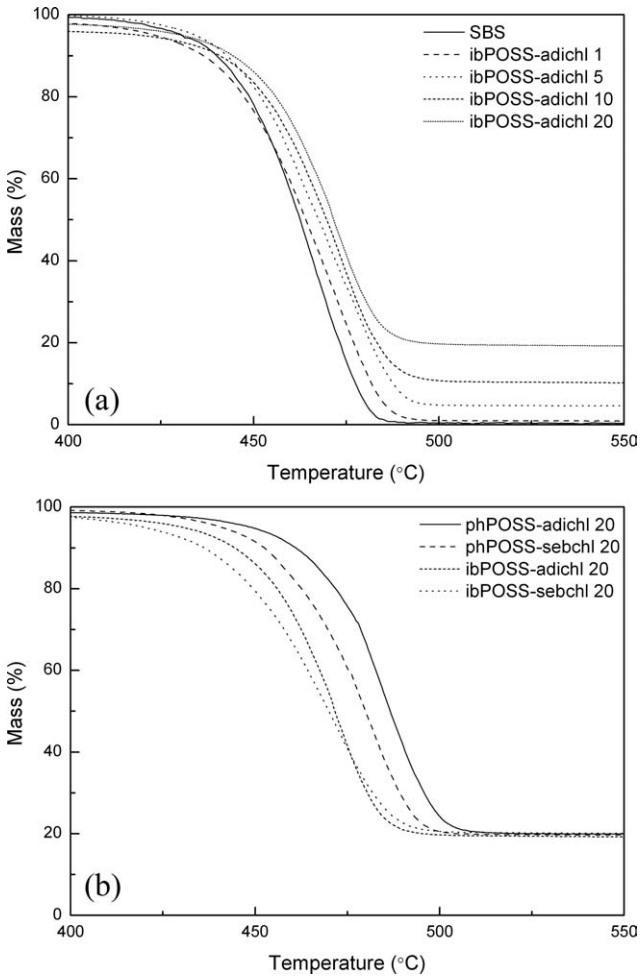

Figure 7 Mass loss versus temperature curves; (a) SBS and SBS-ibPOSS-adichl composites, (b) 20·wt % filled POSS composites.

bonds within the continuous, butadiene phase.[50,52] When dispersed throughout the rubber phase, POSS imparts added stiffness into the matrix by acting as crosslink points and reducing chain mobility.[53,54] This provides thermal stability to the phase upon which the thermal degradation mechanism is dependent. At higher filler loadings (10 and 20·wt %), phenylPOSS composites were observed to be more thermally stable than those containing isobutylPOSS, as shown in Figure 7(b). This is attributed, in part, to the difference in thermal stability between the phenyl and isobutyl "R" compatibilizing groups, with the former possessing greater intrinsic thermal stability.[55,56] A proposed mechanism is that at filler concentrations of 10·wt %and higher, phenyl "R" groups are more effective at reinforcing or "shielding" the butadiene domains than isobutyl groups. Another possibility is that at higher filler loadings, phPOSS segments may be present within the polybutadiene phase.

Composites containing POSS functionalized with adipoyl chloride exhibited greater thermal stability

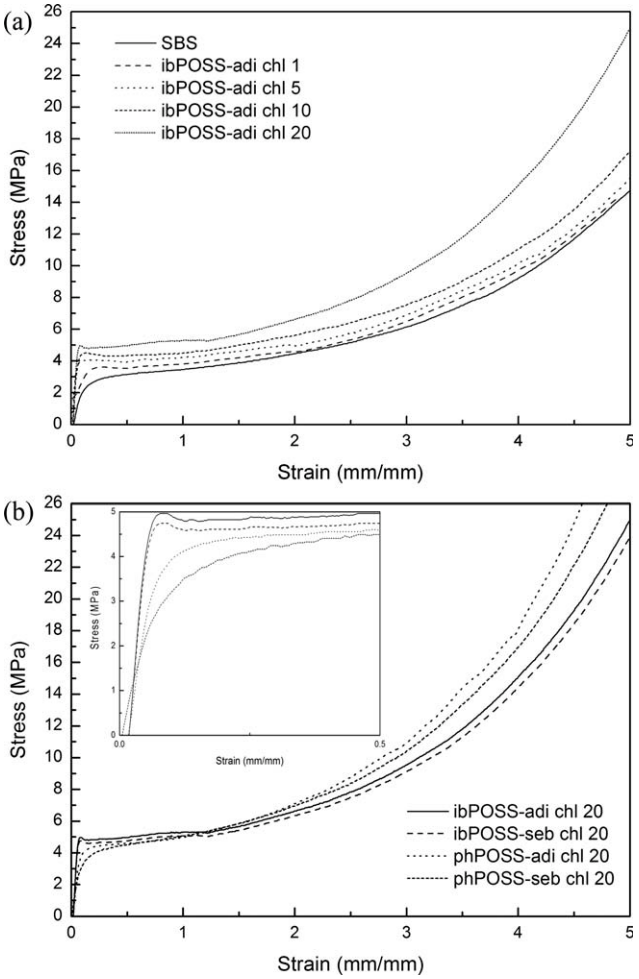

Figure 8 Stress–strain curves of SBS and selected composites; (a) SBS-ibPOSS-adichl composites, (b) 20·wt % filled composites.

than those functionalized with sebacoyl chloride. Several authors have observed similar behavior for materials containing diacyl chlorides with different "bridge" lengths (succinyl, adipoyl, sebacoyl, etc),[57–59] with thermal stability being inversely proportional to alkane chain length. Adipoyl chloride contains a butane "barbell" connecting the two amide groups while sebacoyl chloride contains an octane linkage. As alkane chain length is increased, thermal stability decreased due to the gain in organic fuel for combustion.[60,61] Therefore, the relatively rigid butane linkage of adipoyl chloride will provide greater thermal stability and be less susceptible to thermal degradation than the octane "barbell" of sebacoyl chloride.

Thermomechanical analysis

Stress–strain analysis

The stress–strain curves of SBS and SBS-ibPOSS-adichl composites are presented in Figure 8(a), while the tensile properties are summarized in Table II. All composites exhibited stress–strain curves with similar features. Application of load caused an initial linear increase in strain, due to the occurrence of elastic deformation. This extension continued until reaching a maximum at the yield stress, most notably with increasing ibPOSS-adichl concentration. Increasing the stress past yield caused a brief plateau in strain as the composites enter the nonlinear region and experience viscoelastic flow. Further increase in stress imparted strain hardening into the composites, as strain continued to increase with applied load. Pure SBS displayed a tensile modulus (E) of 26.89 MPa and strength of 3.02 MPa. Addition of POSS had a positive effect on E and strength, reaching maximum values at filler loadings of 20·wt %. The increase is characteristic of the reinforcement ability of POSS. The applied stress was transferred from the SBS matrix to the POSS filler resulting in increased strength and stiffness. This stress-transfer process was aided by sufficient interfacial adhesion between the matrix and filler, achieved through compatibilising "R" groups on the POSS molecules. Furthermore, effective dispersion of the filler throughout the SBS matrix, produced by ultrasonic disruption during composite preparation and confirmed by SEM (refer Fig. 4), contributed to the improved mechanical properties. Filler dispersion promotes an even transfer of stress from the matrix to the reinforcement and prevents the formation of stress concentrations. This mechanism is crucial for enhancing mechanical properties within filler-dispersed composites.

IsobutylPOSS composites exhibited the greatest modulus and strength values. This was attributed to the dispersion of POSS within the polybutadiene

TABLE II
Tensile Mechanical Properties of SBS and SBS-POSS Composites

Material	Tensile modulus (MPa)	Yield strength (MPa)	Strain hardening modulus (MPa)
SBS	26.89	3.02	5.94
ibPOSS-adichl-1	43.67	3.63	6.93
ibPOSS-adichl-5	78.56	4.06	7.21
ibPOSS-adichl-10	86.25	4.52	5.94
ibPOSS-adichl-20	137.08	4.98	7.77
ibPOSS-sebchl-1	41.14	3.36	6.13
ibPOSS-sebchl-5	80.54	3.97	8.00
ibPOSS-sebchl-10	83.70	4.14	7.75
ibPOSS-sebchl-20	115.45	4.75	7.56
phPOSS-adichl-1	37.78	3.13	6.45
phPOSS-adichl-5	62.30	3.48	6.86
phPOSS-adichl-10	74.28	3.82	7.00
phPOSS-adichl-20	94.09	4.46	8.64
phPOSS-sebchl-1	32.27	3.05	8.45
phPOSS-sebchl-5	51.03	3.22	8.25
phPOSS-sebchl-10	59.65	3.54	7.07
phPOSS-sebchl-20	80.12	4.18	9.08

(rubber) phase of the SBS, facilitated by the isobutyl "R" groups on the POSS molecule. The styrene domains within SBS act as crosslinks, restricting the flow of the rubber phase and providing strength and durability. Incorporating POSS into the rubber phase provides additional reinforcement, allowing for greater amounts of stress to be transferred from the polybutadiene. The *E* increased with filler content, ranging from 43.67 and 41.14 MPa for 1·wt % composites of isobutylPOSS-adichl and isobutylPOSS-sebchl, respectively, to 137.08 and 115.45 MPa for their respective 20·wt % counterparts. PhenylPOSS composites exhibited lower E and yield strength values than composites containing isobutylPOSS, due to the phenyl "R" groups on the POSS molecules which provide an affinity toward the glassy, polystyrene segments within the SBS. This reduces the chance of POSS being dispersed throughout the continuous polybutadiene phase and providing adequate reinforcement. As shown in Figure 8(b), POSS functionalized with adipoyl chloride had a greater influence on modulus and yield strength than their sebacoyl chloride counterparts. This was attributed to the difference in "barbell" length of the two molecules. POSS molecules functionalized with adipoyl chloride are bridged by a shorter, less-flexible, and more constrained butane chain segment. This provides greater rigidity and reinforcement than the longer, more-flexible octane chain segment of sebacoyl chloride.

All composites exhibited strain hardening past the yield, due to deformation of the hard (polystyrene) domains and alignment of polymer chains in both segments.[62] As shown in Figure 8(b), phenylPOSS composites displayed higher strain hardening moduli than isobutylPOSS (refer Table I) and supported greater stress levels past the yield. Within elastomers, the glassy components contribute to strain hardening by providing rigidity.[63] Introducing phenylPOSS into the SBS matrix provides additional styrene (hard) domains which increase "hinge length" (the length of rigid-chain units between flexible linkages).[64] IsobutylPOSS composites also exhibited greater strain hardening than pure SBS due to the fillers acting as crosslinks, increasing network density, and encouraging strain delocalization.[65] The tensile results indicate that isobutylPOSS is most effective for improving tensile modulus and strength while phenylPOSS allows for support of greater stress levels following plastic deformation.

Creep-recovery analysis

The creep-recovery curves of SBS and nanocomposites are shown in Figure 9. Several distinctive regions can be observed in the creep-recovery curve of pure SBS with the application and removal of load. The first is the instantaneous increase in strain,

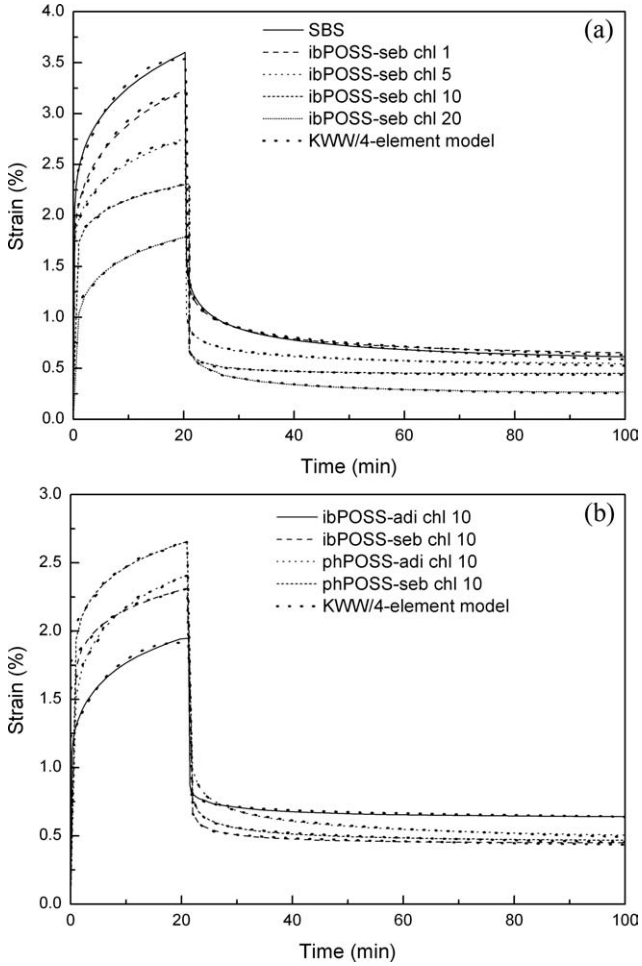

Figure 9 Creep recovery curves of SBS and selected composites; (a) SBS-ibPOSS-sebchl composites, (b) 10·wt % filled composites.

due to the elastic response of the butadiene phase. This is followed by the viscoelastic response, where time-dependent molecular rearrangement occurs. In elastomers, molecular motions involve chain sliding mechanisms, except at entanglements and crosslinks.[66] At times toward the end of the load application period, viscous flow of the polymer is observed. Although the styrene domains provide some resistance against creep deformation, these crosslinks undergo bond cleavage and deformation at sufficient stress levels over extended periods of time.[67] Removal of the load results in a rapid drop in strain response, which is equal to the initial elastic response. The recovery period involves time-dependent molecular relaxations as the polymer attempts to regain original dimensions.[68,69] Since SBS exhibited viscous flow, full recovery is unattainable resulting in permanent deformation.

Creep deformation decreased with increasing POSS content, as displayed in Figure 9(a). This was expected of an elastomer filled with rigid reinforcement. Because of its ceramic silica structure, the

TABLE III
Creep-Recovery Data of SBS and SBS-POSS Composites

Material	E_1 (MPa)	η_1 (MPa s^{-1})	E_2 (MPa)	η_2 (MPa s^{-1})	τ (s)	Permanent deformation (%)
SBS	0.22	67.91	0.35	3.31	9.46	18
ibPOSS-adichl-1	0.25	60.16	0.44	3.60	7.78	21
ibPOSS-adichl-5	0.26	75.43	0.63	3.97	5.37	22
ibPOSS-adichl-10	0.42	92.70	0.73	5.18	6.33	33
ibPOSS-adichl-20	0.51	150.28	0.93	5.60	6.16	39
ibPOSS-sebchl-1	0.26	61.27	0.36	3.49	6.97	20
ibPOSS-sebchl-5	0.27	74.39	0.51	3.91	6.94	20
ibPOSS-sebchl-10	0.39	89.06	0.60	4.38	6.69	25
ibPOSS-sebchl-20	0.48	136.34	0.81	4.86	6.78	34
phPOSS-adichl-1	0.23	62.32	0.41	3.19	8.18	15
phPOSS-adichl-5	0.27	71.68	0.62	3.33	6.30	17
phPOSS-adichl-10	0.34	85.63	0.66	4.18	7.10	21
phPOSS-adichl-20	0.41	102.07	0.69	4.25	6.02	23
phPOSS-sebchl-1	0.21	75.89	0.44	3.07	9.69	18
phPOSS-sebchl-5	0.23	79.19	0.51	3.54	7.67	19
phPOSS-sebchl-10	0.26	82.92	0.52	3.48	7.30	18
phPOSS-sebchl-20	0.36	85.36	0.60	4.07	6.00	18

presence of POSS imparts stiffness into the matrix and aids in restricting the molecular motions of the polybutadiene chains, resulting in a lower susceptibility to deform under a given load. Furthermore, the compatibilizing organic groups on the POSS encourage interaction and adhesion between the matrix and filler, contributing to nanocomposite resistance to deformation. At higher POSS loadings (10 and 20·wt %), nanocomposites exhibited flatter creep curves with a lower gradient, indicating a decrease of deformation of the viscous component. Nanocomposites containing isobutylPOSS exhibited less deformation than their phenylPOSS counterparts due to filler phase compatibility, which was in agreement with the stress–strain results. Since the polybutadiene chains which make up the rubbery, continuous phase experience molecular rearrangement and motions under stress, it is more effective to disperse filler throughout this phase to reduce deformation.

When comparing the curves of the adipoyl and sebacoyl chloride POSS composites [Fig. 9(b)], a significant difference in creep behavior is evident. Nanocomposites containing POSS functionalized with adipoyl chloride showed considerably less creep and deformation than those functionalized with sebacoyl chloride. This occurrence can be attributed to the difference in 'barbell' length for the POSS molecules. The shorter, more-rigid butane "barbell" of adipoyl chloride provides greater resistance to creep and deformation, compared to its flexible octane (sebacoyl chloride) counterpart. This observation is in good correlation with the stress–strain results and suggests that the bridge length between two POSS molecules can impart some physical constraints to dimensional stability.

The parameters of the four-element model were calculated for the creep components of SBS and the nanocomposites, which are presented in Table III. SBS exhibited the greatest strain response under load while the POSS nanocomposites were found to lessen the creep strain response, providing stearic resistance to both elastic and viscous contributions. The Maxwell modulus (E_1) of SBS was 0.22 MPa, which was increased with POSS content particularly at higher contents (5–20·wt %), confirming that the nano-sized particulate fillers influenced the flow characteristic of the SBS matrix. The Maxwell viscosity (η_1) followed similarly with an increase with POSS content. These results confirm the addition aids in restraining deformation, even more so at higher amounts of POSS. This is attributed to the dispersion of nano-particulates and phase compatibility with the isobutyl or phenyl functionalization and phase preferentiation, even with the formation of aggregates at higher content. Nanocomposites containing ibPOSS exhibited larger Maxwell component (E_1 and η_1) values than their phenylPOSS counterparts functionalized with the same diacyl chloride. Similarly, composites with adipoyl chloride functionalized POSS yielded higher values than sebacoyl chloride functionalized POSS. All materials displayed a certain proportion of unrecovered strain that is characteristic of viscous, amorphous materials such as SBS. This is due to chain entanglement slippage and detachment of styrene domains from the polybutadiene rubber-phase that occurs during the application of load. Permanent deformation increased with POSS concentration, with nanocomposites containing adipoyl chloride-isobutyl-POSS displaying the largest values. Higher concentrations of filler, such as POSS, restrict the relaxation of SBS chains, causing irreversible chain slippage and unraveling. The Voigt viscosity (η_2) was observed to increase with POSS content, suggesting an increase in resistance of the SBS chains to uncoil.

TABLE IV
KWW Parameters of SBS and SBS-POSS Composites

Material	*A*	β	τ (s)
SBS	3.18	0.14	35.74
ibPOSS-adichl-1	3.17	0.08	29.58
ibPOSS-adichl-5	2.80	0.08	18.77
ibPOSS-adichl-10	2.34	0.04	9.51
ibPOSS-adichl-20	1.08	0.04	6.33
ibPOSS-sebchl-1	4.34	0.09	30.11
ibPOSS-sebchl-5	3.11	0.07	22.78
ibPOSS-sebchl-10	1.95	0.05	17.70
ibPOSS-sebchl-20	1.97	0.12	12.44
phPOSS-adichl-1	3.97	0.09	32.98
phPOSS-adichl-5	3.93	0.08	23.98
phPOSS-adichl-10	3.16	0.09	15.72
phPOSS-adichl-20	2.45	0.09	9.33
phPOSS-sebchl-1	4.33	0.08	35.98
phPOSS-sebchl-5	4.03	0.07	27.73
phPOSS-sebchl-10	2.70	0.05	11.77
phPOSS-sebchl-20	2.40	0.10	12.63

The retardation time (τ) is required to determine η_2 and is defined by Eq. (5).

$$\tau = \frac{\eta_2}{E_2} \tag{5}$$

It is the time required for the Voigt element (viscoelastic component) to recover to 63.21% (or $1 - 1/e$) of its total deformation. Although real polymers display a range of retardation times due to their molecular weight distribution, a single τ provides a quick and simple estimate for how changes in structure can influence behavior.[70] Increasing the POSS content caused the τ to decrease, suggesting that the nanocomposites become more solid-like in behavior at higher filler concentrations. Similarly, highly filled composites exhibited flatter recovery curves, indicating a faster recovery of the viscoelastic and elastic components. Nanocomposites containing phenylPOSS displayed slightly longer τ than their isobutylPOSS counterparts with the same "barbell" length. When rubbery, polybutadiene chains are highly stretched under an applied load, phenylPOSS molecules can become detached from the glassy, styrene domains for which they have an affinity. This can lead to dissimilar block-mixing occurring in interfacial regions, causing an increase in permanent deformation.[67] Nanocomposites functionalised with adipoyl chloride yielded shorter τ than those functionalized with sebacoyl chloride. This was attributed to the increased restrictions placed on segmental motions for relaxation by the stiffer, butane bridge, causing the material to behave in a more solid-like nature. These results correlate well to the behavior observed in the creep component and stress–strain analysis.

To further examine relaxation behavior, the KWW stretched exponential function was applied to SBS and the nanocomposites. The results are presented in Table IV. In fitting the function, the pre-exponential constant and relaxation time decreased with increasing POSS content. This was to be expected since the relaxation provides an indication of the degree of mobility molecules within the polymer possess. The decreased relaxation time at higher POSS concentrations is indicative of the solid-like behavior highly-filled nanocomposites exhibit and is in agreement with the creep data obtained using the four-element model. Correspondingly, the shape fitting parameter β changed with POSS content. The value of β is influenced by various factors, including structure, the presence of fillers, crosslinks, and crystallinity.[71] These observations strongly suggest that the nanocomposites experience restricted flow, attributed to the incorporation of functionalized-POSS.

Modulated force-thermomechanometry

Figure 10(a) shows the storage modulus (E') of SBS and selected nanocomposites. At temperatures below −100°C the polymer was in a glassy state, with the modulus remaining fairly constant at ~ 2.0 GPa. The modulus began to decrease as it approached the α glass-rubber transition of the rubbery, butadiene phase. Heating above the glass transition temperature (T_g) provides sufficient activation energy for rotation about bonds in segments of the polymer, causing a loss in material rigidity. Following this transition, the modulus of SBS briefly plateaued at −30°C, maintaining an E' value of ~ 0.03 GPa. Increasing the temperature caused a second drop in modulus as the glassy, styrene phase of SBS underwent the β glass-rubber transition. At higher temperatures (>110°C), the styrene segments flow after undergoing the transition and are unable to continue to provide the SBS with structural integrity and reinforcement. As a result, the polymer lacks any rigidity, becoming very viscous and liquid-like.

Nanocomposites containing POSS displayed higher E' values than pure SBS. As shown in Figure 10(a), the E' modulus reached a maximum at POSS concentrations of 20·wt %, with SBS-ibPOSS-adichl 20 and SBS-ibPOSS-sebchl 20 exhibiting E' values of 5.3 and 5.0 GPa at −90°C, respectively. Similar observations were recorded at the plateau before the polystyrene transition, with maximum E' values of 0.24 and 0.21 GPa for SBS-ibPOSS-adichl 20 and SBS-ibPOSS-sebchl 20, respectively, at 10°C. These results are indicative of the additional stiffness imparted by POSS. The highest modulus values were exhibited by composites containing isobutylPOSS functionalized with adipoyl chloride, attributed to influence of phase preference and filler stiffness, respectively, on

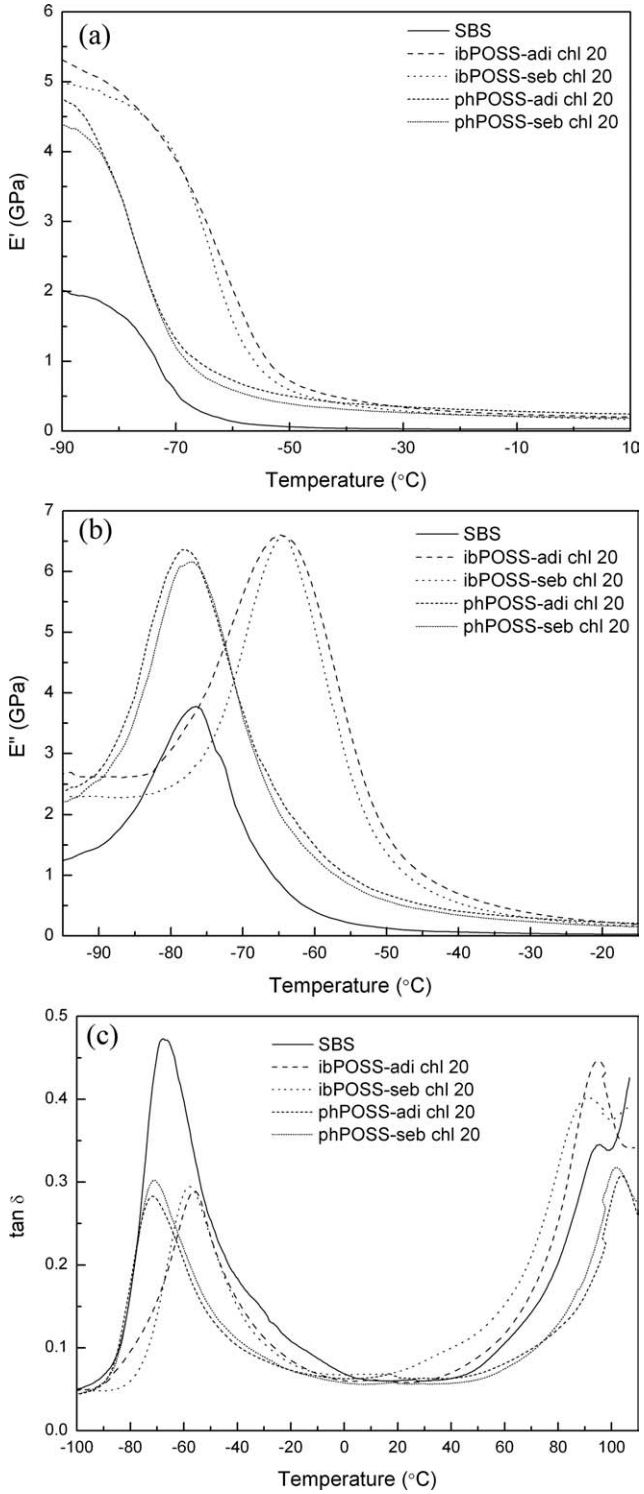

Figure 10 mf-TM curves of SBS and composites filled with 20·wt % functionalized POSS; (a) storage modulus, (b) loss modulus, (c) tan δ.

mechanical properties. This influence of filler structure on mechanical properties is in agreement with behavior observed in creep-recovery analysis. At temperatures above the α (butadiene) transition, the decrease in E' modulus was reduced when compared with pure SBS, while an increase in E' reduction rate was observed at temperatures above the β (styrene) transition.

The loss modulus (E'') of SBS and nanocomposites is shown in Figure 10(b), while T_g values are summarized in Table V. The T_g is determined by the peak of the E'' curve (E''_{max}), since that is where maximum heat dissipation occurs. Pure SBS displays two curves, at −75 and 88°C. These peaks correspond to the T_g of the butadiene and styrene phases, respectively. Addition of POSS caused the T_g to increase in, reaching a maximum at 20·wt %. The increase in glass transition temperature is attributed to the ability of the functionalized-POSS to restrict molecular motions of the polymer chains, causing the material to become less flexible. As summarized in Table IV, composites containing isobutylPOSS displayed the greatest increase in T_g for the butadiene phase, with ibPOSS-adichl 20 and ibPOSS-sebchl 20 yielding T_g values of −65 and −64°C, respectively. Similarly, materials filled with phenylPOSS exhibited higher T_g values for the polystyrene transition than their isobutylPOSS counterparts. This behavior suggests that the compatibilising groups are providing an affinity for their corresponding phases, allowing the POSS to disperse throughout and entangle within a particular phase within the SBS. At concentrations of 10 and 20·wt % phenylPOSS reduced the T_g of polybutadiene. Because of the limited volume of polymer available for the phenylPOSS to disperse throughout, at higher filler loadings (10 and 20·wt %) small fractions of phenylPOSS may be present within the soft, polybutadiene domains, reducing the T_g.[36]

Composites functionalized with adipoyl chloride displayed higher T_g values than those treated with sebacoyl chloride. This was due to the structure of adipoyl chloride's butane chain segment, which allows for additional restraint on molecular motions. Composites exhibited glass transitions over a larger temperature range, as indicated by the broader E''

TABLE V
Glass Transition Data of SBS and Composites Filled with 5 and 20 wt % POSS

	T_g from E'' max (°C)		T_g from tan δ max (°C)	
Material	Butadiene phase	Styrene phase	Butadiene phase	Styrene phase
SBS	−75	88	−67	95
ibPOSS-adichl-5	−72	88	−65	94
ibPOSS-adichl-20	−64	86	−56	93
ibPOSS-sebchl-5	−73	88	−65	95
ibPOSS-sebchl-20	−65	82	−58	90
phPOSS-adichl-5	−74	91	−69	98
phPOSS-adichl-20	−78	97	−72	104
phPOSS-sebchl-5	−75	90	−68	97
phPOSS-sebchl-20	−77	94	−70	102

peaks. The increase in peak breadth is attributed to an increase in the segmental relaxation times of the matrix.[72] Peak breadth was observed to increase with POSS concentration, reaching maximum values at loadings of 10 and 20·wt %, suggesting an increase in the relaxation time due to segmental constraints, including polymer chain coupling and polymer-POSS interactions.

The loss tangent (tan δ) of SBS and several nanocomposites is shown in Figure 10(c). The maximum of the tan δ curve can be used to determine T_g, although the E'' maximum is shown to be more consistent with other determinations of T_g. The tan δ were ~ 6–8°C higher than T_g obtained from loss modulus curves (refer Table V). The glass transition temperatures obtained from the loss tangent maximum displayed similar trends to those obtained from E''_{max}. Nanocomposites containing isobutylPOSS showed a reduction in butadiene-phase peak height, with 20·wt % exhibiting the greatest reduction. Conversely, increasing the isobutylPOSS concentration caused an increase in the styrene-phase peak. The amplitude of the tan δ peak provides an indication of the number of kinetic units mobile enough to contribute to the glass transition.[73] The decrease in peak intensity indicates that isobutylPOSS molecules restrict motions of polymer chains within the butadiene phase, as indicated by the isobutylPOSS nanocomposites displaying T_g values higher than SBS. The increase peak height of the styrene phase suggests an increase in free volume and plasticizing effect on the glassy domains, leading to composites displaying T_g values lower than SBS. The addition of phenylPOSS similarly caused a decrease in the butadiene-phase peak, which was expected since the styrene domains within SBS provide the polymer with rigidity and structure.

Adipoyl chloride composites exhibited slightly lower tan δ peak heights than their sebacoyl chloride counterparts. This was attributed to composites containing stiffer, adipoyl chloride-functionalized POSS behaving more solid-like than those with sebacoyl chloride POSS, resulting in decreased dampening properties. The damping ability of a filled polymer system is believed to be influenced by two factors: (a) the amount of free volume, (b) internal friction between the filler and matrix and between the filler particles themselves across the glass transition region.[74] The latter increases as the number of chain movements become greater, leading to an increase in damping ability. Composites containing sebacoyl chloride-functionalized POSS are able to experience greater chain motion due to the flexible structure of the filler, experiencing greater internal friction than their adipoyl chloride counterparts and subsequently exhibiting enhanced dampening properties. As with the E'' curves, peak broadening of the tan δ curves was observed at higher filler loadings. Since the peak breadth is an indication of structural heterogeneity, the wider peaks suggest an increase in segmental relaxation time due to increased SBS-POSS interactions. The broader peaks are also indicative of the aforementioned increase in damping and internal friction.

CONCLUSION

SBS-POSS nanocomposites were prepared via physical blending. Prior to their dispersion throughout the polymer matrix, POSS molecules were successfully functionalized with adipoyl and sebacoyl chloride as indicated by FTIR. Agglomerate size increased with filler content, due to increased interactions between the POSS particles. The morphology of the nanocomposites was dependent on the organic substituent groups on the POSS cages, with the amount of filler aggregation being dependent on the relative volume of butadiene or styrene phase to disperse throughout. The polydispersity of SBS increased with filler concentration. IsobutylPOSS was observed to be confined within the polybutadiene domains and did not change the cylinder morphology of SBS. The increased d spacing values of phenylPOSS composites suggests the filler expands polystyrene domains within the matrix, leading to an increase in interdomain distance.

IsobutylPOSS had the greatest influence on thermal stability at filler loadings of 1–5·wt %, due to its incorporation into the thermally-sensitive polybutadiene phase. At concentrations of 10 and 20·wt %, phenylPOSS composites exhibited greater thermal stability, corresponding to the increased presence of more-stable phenyl groups. POSS functionalized with adipoyl chloride exhibited a marginally better influence on thermal stability than its sebacoyl chloride counterpart, due to the butane "barbell" (alkane chain length) being less susceptible to thermal degradation than octane. The tensile modulus (E), yield strength and strain hardening of the nanocomposites increased with filler content. Creep deformation decreased and permanent strain increased with POSS content, due to the restricted molecular motions caused by filler. Incorporation of POSS increased the storage modulus (E'), loss modulus (E'') and glass transition temperature (T_g). Three factors contributed to the mechanical properties of the nanocomposites; (a) POSS concentration, (b) the phase which the POSS was dispersed throughout, (c) the architecture of the dumbbell-shaped POSS, specifically the "barbell" length.

References

1. Tsubokawa, N.; Hosoya, M. React Polym 1991, 14, 33.
2. Pereira, C.; Silva, A. R.; Carvalho, A. P.; Pires, J.; Freire, C. J Mol Catal A Chem 2008, 283, 5.

3. Jeon, Y. M.; Lim, T. H.; Lee, C. W.; Cheon, J. W.; Gong, M. S. J Ind Eng Chem 2007, 13, 518.
4. Winnik, F. M.; Keoshkerian, B.; Fuller, J. R.; Hofstra, P. G. Dye Pigment 1990, 14, 101.
5. Bianchi, C.; Noor, S.; Mirley, C. L.; Bauer, R.; Yener, D. US Patent 7,479,324, 2009.
6. Newman, J. D. S.; Roberts, J. M.; Blanchard, G. J Anal Chem 2007, 79, 3448.
7. Majewski, P.; Thierry, B. Crit Rev Solid Stat Mater Sci 2007, 32, 203.
8. DeArmitt, C.; Wheeler, P. Plast Add Comp 2008, 10, 36.
9. Scott, D. W. J Am Chem Soc 1946, 68, 356.
10. Wheeler, P. A.; Fu, B. X.; Lichtenhan, J. D.; Weitao, J.; Mathias, L. J. J Appl Polym Sci 2006, 102, 2856.
11. Al Ghatta, H.; Abbenhuis, H. C. L. Organization, WIPO Patent 009,707, 2008.
12. Froehlich, J. D.; Young, R.; Nakamura, T.; Ohmori, Y.; Li, S.; Mochizuki, A.; Lauters, M.; Jabbour, G. E. Chem Mater 2007, 19, 4991.
13. Hartmann-Thompson, C.; Keeley, D.; Pollock, K. M.; Dvornic, P. R.; Keinath, S. E.; Dantus, M.; Gunaratne, T. C.; LeCaptain, D. J Chem Mater 2008, 20, 2829.
14. Hybrid Plastics™ POSS®. Chem Catalog. Hybrid Plastics: Hattiesburg, 2008; p 36.
15. Strachota, A.; Kroutilová, I.; Kovářová, J.; Matějka, L. Macromolecule 2004, 37, 9457.
16. Lichtenhan, J. D.; Vu, N. Q.; Carter, J. A.; Gilman, J. W.; Feher, F. J Macromol 1993, 26, 2141.
17. Zhang, W.; Müller, A. H. E. Polymer 2010, 51, 2133.
18. Bian, Y.; Mijovic, J. Macromolecule 2009, 42, 4181.
19. Lu, C. H.; Wang, J. H.; Chang, F. C.; Kuo, S. W. Macromol Chem Phys 2010, 211, 1339.
20. Romo-Uribe, A.; Mather, P. T.; Haddad, T. S.; Lichtenhan, J. D. J Polym Sci B Polym Phys 1998, 36, 1857.
21. Pyun, J.; Matyjaszewski, K.; Wu, J.; Kim, G. M.; Chun, S. B.; Mather, P. T. Polymer 2003, 44, 2739.
22. Mantz, R. A.; Jones, P. F.; Chaffee, K. P.; Lichtenhan, J. D.; Gilman, J. W.; Ismail, I. M. K.; Burmeister, M. J. Chem Mater 1996, 8, 1250.
23. Tsuchida, A.; Bolln, C.; Sernetz, F. G.; Frey, H.; Mülhaupt, R. Macromolecule 1997, 30, 2818.
24. Su, X.; Xu, H.; Deng, Y.; Li, J.; Zhang, W.; Wang, P. Mater Lett 2008, 62, 3818.
25. Su, X.; Guang, S.; Xu, H.; Liu, X.; Li, S.; Wang, X.; Deng, Y.; Wang, P. Macromolecule 2009, 42, 8969.
26. Kim, B. S.; Mather, P. T. Polymer 2006, 47, 6202.
27. Lee, W.; Ni, S.; Deng, J.; Kim, B. S.; Satija, S. K.; Mather, P. T.; Esker, A. R. Macromolecule 2007, 40, 682.
28. Mather, P. T.; Kim, B. S.; Qing, G.; Liu, C. US Patent 20040024098, 2004.
29. Adhikari, R.; Michler, G. H. Prog Polym Sci 2004, 29, 949.
30. Park, C.; Yoon, J.; Thomas, E. L. Polymer 2003, 44, 6725.
31. Balsamo, V.; Lorenzo, A. T.; Müller, A. J.; Corona-Galvan, S.; Trillo, L. M. F.; Quiteria, V. R. S. In Block Copolymers in Nanoscience; Lazzari, M.; Liu, G.; Lecommandoux, S., Ed.; Wiley-VCH: Weinheim, 2006; Chapter 16, p 367–390.
32. Adhikari, R.; Henning, S.; Lebek, W.; Godehardt, R.; Ilisch, S.; Michler, G. H. Macromol Symp 2006, 231, 116.
33. Choi, S. S. J Appl Polym Sci 2002, 85, 385.
34. Praveen, S.; Chattopadhyay, P. K.; Albert, P.; Dalvi, V. G.; Chakraborty, B. C.; Chattopadhyay, S. Compos A 2009, 40, 309.
35. Chen, Z.; Feng, R. Polym Compos 2009, 30, 281.
36. Drazkowski, D. B.; Lee, A.; Haddad, T. S.; Cookson, D. J Macromol 2006, 39, 1854.
37. Drazkowski, D. B.; Lee, A.; Haddad, T. S. Macromolecule 2007, 40, 2798.
38. Fu, B. X.; Lee, A.; Haddad, T. S. Macromolecule 2004, 37, 5211.
39. Williams, G.; Watts, D. C. Trans Faraday Soc 1970, 66, 80.
40. Fancey, K. S. J Polym Eng 2001, 21, 489.
41. Nunes, S. C.; de Zea Bermudez, V.; Cybinska, J.; SáFerreira, R. A.; Legendziewicz, J.; Carlos, L. D.; Silva, M. M.; Smith, M. J.; Ostrovskiie, D.; Rocha, J. J Mater Chem 2005, 15, 3876.
42. Coates, J. In Encyclopedia of Analytical Chemistry; Meyer, R. A., Ed.; Wiley: Chichester, 2000; p 10815.
43. Botelho, E. C.; Scherbakoff, N.; Rezende, M. C.; Kawamoto, A. M.; Sciamareli, J. Macromolecule 2001, 34, 3367.
44. Romo-Uribe, A. Revista Mexicana De Física 2007, 53, 171.
45. Causin, V. In Rubber Nanocomposites: Preparation, Properties, and Applications; Thomas, S.; Stephen, R., Eds.; Wiley: Singapore, 2010, p 425–497.
46. Wu, J. H.; Li, C. H.; Wu, Y. T.; Leu, M. T.; Tsai, Y. Compos Sci Technol 2010, 70, 1258.
47. Schmidt, G.; Malwitz, M. M. Curr Opin Coll Interfac Sci 2003, 8, 103.
48. Turssi, C. P.; Ferracane, J. L.; Vogel, K. Biomaterials 2005, 26, 4932.
49. Boydağ, F.Ş.; Mamedov, S. V.; Alekperov, V. A.; Lenger Özcanli, Y. Optic Spectro 2003, 95, 225.
50. Xu, J.; Zhang, A.; Zhou, T.; Cao, X.; Xie, Z. Polym Degrad Stab 2007, 92, 1682.
51. Liu, Y. R.; Huang, Y. D.; Liu, L. Polym Degrad Stab 2006, 91, 2731.
52. Lu, L.; Yu, H.; Wang, S.; Zhang, Y. J Appl Polym Sci 2009, 112, 524.
53. Sim, L. C.; Ramanan, S. R.; Ismail, H.; Seetharamu, K. N.; Goh, T. J Thermochim Acta 2008, 430, 155.
54. Zhang, J.; Feng, S.; Ma, Q. J Appl Polym Sci 2003, 89, 1548.
55. Shirai, M.; Shimoji, S.; Ishii, T. IEEE Trans Elect Insul 1977, EI-12, 272.
56. Fina, A.; Tabuani, D.; Carniato, F.; Frache, A.; Boccaleri, E.; Caminoa, G. Thermochim Acta 2006, 440, 36.
57. Ebadi, H.; Mehdipour-Ataeib, S. Chin J Polym Sci 2010, 28, 29.
58. Kim, J. H.; Won, D. S.; Lee, J. Y. Bull Kor Chem Soc 2008, 29, 181.
59. Podkościelny, W.; Wdowicka, D. J Appl Polym Sci 1988, 35, 1779.
60. Olin, J. B.; Wiese, H. C.; Sage, B. H. J Chem Eng Data 1961, 6, 372.
61. Koch, B. J Synth Lube 1990, 6, 275.
62. Huy, T. A.; Adhikari, R.; Michler, G. H. Polymer 2003, 44, 1247.
63. Cerrada, M. L.; de la Fuente, J. L.; Fernández-García, M.; Madruga, E. Polymer 2001, 40, 4647.
64. Haward, R. N. Macromolecule 1993, 26, 5860.
65. Kierkels, J. T. A. PhD Thesis, Technische Universiteit Eindhoven, Eindhoven, 2006.
66. Mostafa, A.; Abouel-Kasem, A.; Bayoumi, M. R.; El-Sebaie, M. G. Mater Des 2009, 30, 2721.
67. Blackwell, R. I.; Mauritz, K. A. Polym Adv Technol 2005, 16, 212.
68. Spoljaric, S.; Genovese, A.; Shanks, R. A. Compos A 2009, 40, 791.
69. Genovese, A.; Shanks, R. A. Macromol Mater Eng 2007, 292, 184.
70. Menard, K. P. Dynamic Mechanical Analysis: A Practical Introduction; CRC Press: New York, 2008.
71. Kaminski, D.; Shanks, R. In 32nd Condensed Matter and Materials Meeting, Wagga Wagga, Australia, 2008.
72. Verghese, K. N. E.; Jensen, R. E.; Lesko, J. J.; Ward, T. C. Polymer 2001, 42, 1633.
73. Kennedy, J. E.; Lyons, J. G.; Geever, L. M.; Higginbotham, C. L. Mater Sci Eng C 2009, 29, 1655.
74. Trakulsujaritchok, T.; Hourston, D. J Eur Polym J 2006, 42, 2968.